COMMUNICATION

Individually Position-Addressable Metal-Nanofiber Electrodes for Large-Area Electronics

*Yeongjun Lee, Tae-Sik Kim, Sung-Yong Min, Wentao Xu, Su-Hun Jeong, Hong-Kyu Seo, and Tae-Woo Lee**

Fabrication of nano- or sub-microsized electrodes is essential for reduction of the size of electronic devices. Except for expensive and complex vacuum deposition processes, methods to fabricate nano- or sub-microsized electrodes include using synthesized metal nanowires (NWs),[1–3] printed electrodes using metal inks,[4–8] and electrospun metal nanofiber (NF) mats.[9–16] Although metal NWs and electrospun metal NFs are sufficiently small, and have excellent electrical properties that qualify them for use in electronic applications,[1–3,9–16] conducting films that consist of randomly dispersed metal NWs or non-woven metal NF mats have been mainly evaluated for use in sheet-type transparent electrodes of optoelectronic devices such as organic light-emitting diodes and solar cells,[2,12–14] because precise positioning and large-scale alignment of individual metal NWs or metal NF mats for uniformly aligned electrode arrays are difficult tasks. Conventional printing methods that use Ag ink are frequently used for printed electronics based on low process cost and simple steps,[4–8] but have limited resolution (drop-on-demand-type jet printing) or cause contamination and defects during transfer of patterns from stamp to substrate (roll or stamp printing methods). Moreover, although Ag electrodes have diverse advantages of favorable electrical features and chemical stability, the high cost of Ag is a big obstacle to large-scale industrial applications of these electrodes. An alternative material is Cu, which has similar resistivity of 1.68 μΩ cm compared with Ag (1.59 μΩ cm) but is less than 1/100 as expensive as Ag, so demand for Cu electrodes is increasing rapidly.[5–7,10–12,17–20] Therefore, individually position-addressable large-scale-aligned Cu NF electrode array printing with desired orientation and position is necessary; it will achieve direct printing of uniformly aligned extremely small nanoelectrode arrays in large-area. Furthermore, compared to the transmittance of conventional transparent electrodes, individually controlled invisible nanoscale metal fibers can not only be used itself as nanoelectrodes but also generate highly transparent nano-grid electrodes for large-area electronics.

Electro-hydrodynamic nanowire printing (ENP) has been used to fabricate highly aligned organic semiconducting nanowires for large-area organic nanowire transistor arrays and complementary inverter circuit arrays.[21,22] Here, we demonstrate use of ENP to print an individually position-addressable, large-scale-aligned Cu NF array, and fabrication of an organic field-effect transistor (FET) array based on individual Cu NF electrodes. Resistivity of a single-stranded Cu NF was 14.1 μΩ cm, which is only 8.3 times higher than that of bulk Cu (1.68 μΩ cm). On the basis of good electrical property, a bottom-contact pentacene FET with Cu NFs as source/drain (S/D) electrodes was fabricated and showed a maximum carrier mobility μ_{sat} = 0.16 $cm^2\ V^{-1}\ s^{-1}$ (average $\mu_{sat} \approx 0.1 \pm 0.02\ cm^2\ V^{-1}\ s^{-1}$), which is ca. 25 times greater than that of pentacene FET fabricated using vacuum-deposited Cu film electrodes ($\mu_{sat} \approx 0.006 \pm 0.0009\ cm^2\ V^{-1}\ s^{-1}$). Moreover, parallel Cu NF arrays with a regular line spacing of 300 μm have a high transmittance (ca. 98%) in the entire visible range due to a sub-micrometer diameter of 710 nm.

To fabricate (**Figure 1**) an aligned Cu NF array, we examined many kinds of viscous binding polymers and Cu precursors to find the optimum composition of the solution (Table S1, Supporting Information). High-molecular-weight poly(vinylpyrollidone) (PVP) and Cu(II) trifluoroacetate ($Cu(CO_2CF_3)_2$) were added to a mixture of N,N-dimethylformamide (DMF) and tetrahydrofuran (THF) as solvents. Then ENP was used to print a PVP/($Cu(CO_2CF_3)_2$) composite NF array on the substrate at a high speed of 58.3 cm s^{-1} (see Experimental Section). Two steps are needed to convert the PVP/$Cu(CO_2CF_3)_2$ composite NFs to Cu NFs (Figure 1). The first step is to decompose the polymer and precursor components at 500 °C for 1 h in ambient condition to leave CuO NFs. The second step is to reduce CuO NFs to Cu NFs at 300 °C for 1 h under H_2. Before the calcination process, PVP/$Cu(CO_2CF_3)_2$ composite NF had a smooth surface and circular cross section with average diameter of 710 ± 90 nm (**Figure 2**a and Figure S1, Supporting Information). The energy-dispersive X-ray spectroscopy (EDS) spectrum (Figure 2a) showed a C peak that originated from the polymer; as well as additional Cu, O, and F peaks that originated from the precursor; and a sharp Si peak that originated from the native silicon wafer substrate. After the first calcination at 500 °C in air, the NF collapsed due to decomposition of polymer and precursor (Figure 2b), and its surface became grainy caused by formation of CuO grains. In the EDS spectrum, the C peak almost disappeared because of polymer decomposition, but the O peak remained and was sharper than before the calcination, due to the formation of CuO grains (Figure 2b). After the second calcination, the grainy surface of the NF was not changed much (Figure 2c), but the intensity of the O peak in the EDS spectrum of the Cu NF decreased (Figure 2c); this change indicates that the CuO

Y. Lee, T.-S. Kim, S.-Y. Min, Dr. W. Xu, S.-H. Jeong, H.-K. Seo, Prof. T.-W. Lee
Department of Materials Science and Engineering
Pohang University of Science and Technology (POSTECH)
Pohang, Gyungbuk 790–784, Republic of Korea
E-mail: twlee@postech.ac.kr

DOI: 10.1002/adma.201403559

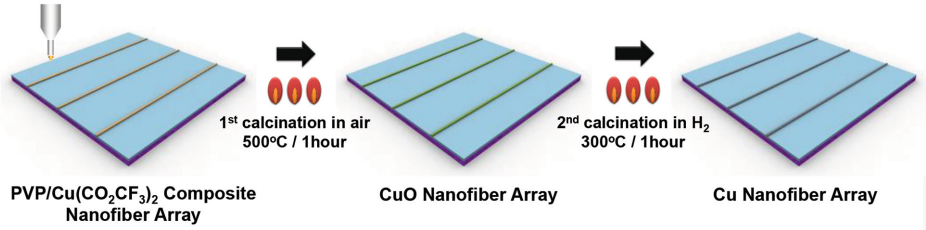

Figure 1. Schematic illustration of fabrication process for Cu NF array. A well-aligned PVP/$Cu(CO_2CF_3)_2$ composite NF array printed by ENP turned into Cu NF array through two steps of calcination processes.

NFs were reduced to Cu NFs. X-ray diffraction (XRD) supports that CuO inside NFs was turned into Cu at higher temperature than 300 °C for at least 1 h under H_2 condition (Figure S2, Supporting Information). Scanning electron microscope (SEM) images (Figure 2d) show aligned composite NFs with constant spacing of 100 μm and intended orientations (i.e., parallel pattern or grid pattern) and finally we achieved parallel and perpendicular patterns of Cu NF arrays (Figure 2e). The parallel patterns of Cu NF arrays with constant spacing of 300 μm on the glass substrate showed very high transmittance (ca. 98%) in the entire visible range (Figure 2f) and were fully transparent because the sub-micrometer-sized patterns were not distinguishable by the naked eye. Conventional vacuum-deposited Cu thin-film transistor electrodes (area: 1.5 mm × 1.6 mm for source–drain electrodes; channel length: 100 μm) deposited using a metal shadow mask (Cu film thickness: 150 nm) are not transparent, so light cannot pass through them (see Figure S3 in the Supporting Information for Cu film device arrays). These extremely transparent metal nanofiber array electrodes can be applicable to various transparent optoelectronics such as transparent displays and solar cells.

The current–voltage (I–V) characteristics of a single Cu NF which was aligned between two Au electrodes with a gap of 100 μm (**Figure 3**) shows clear Ohmic contact with Au, and resistivity of 14.1 μΩ cm which is only 8.3 times higher than that of bulk Cu (1.68 μΩ cm), and is lower than that of the previously reported electrospun Cu NF (120 μΩ cm).[10] The higher resistivity of Cu NFs compared with that of single crystalline Cu NWs (1.18 μΩ cm)[23] mainly comes from the grainy polycrystalline structure (Figure S4, Supporting Information). High-resolution transmission electron microscopy (HRTEM) shows a typical polycrystalline morphology with a clear Moiré fringe and different crystal lattice orientations (Figure S4b, Supporting Information). Ultra-thin surface oxide species on the Cu NFs caused by the instability of Cu in ambient conditions also degrades the electrical conductivity of Cu NFs. Although it has a slightly higher resistivity than bulk Cu, the printed single-stranded Cu NF can be used for the nanoelectrodes of various electronic devices.

To prove the feasibility of our large-scale-aligned Cu NF arrays as individual electrodes of general electronic devices, we fabricated bottom-contact pentacene FET arrays that used individual single-stranded Cu NFs as S/D nanoelectrodes (**Figure 4**a). PVP/$Cu(CO_2CF_3)_2$ composite NF arrays were printed on Si/SiO_2 (300 nm) substrate and calcinated to Cu NFs. To ensure that the measuring tip of the probe station

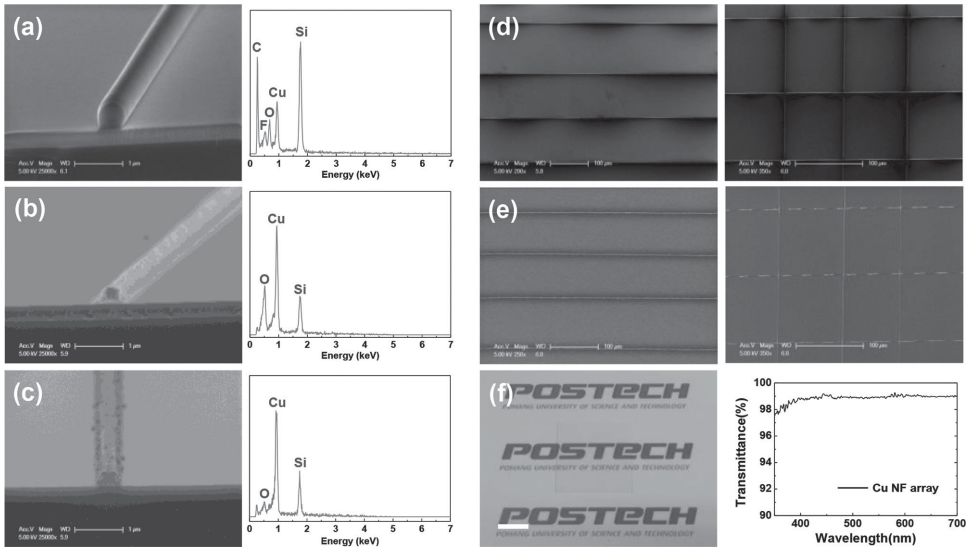

Figure 2. SEM images and EDS spectra of: a) a PVP/$Cu(CO_2CF_3)_2$ composite NF, b) a CuO NF, and c) a Cu NF (scale bar: 1 μm). SEM images of parallel and perpendicular patterns of: d) PVP/$Cu(CO_2CF_3)_2$ composite NF and e) Cu NF (scale bar: 100 μm). f) Digital image of parallel patterns of Cu NF array with constant spacing of 300 μm on the glass substrate (2.5 cm × 2.5 cm), scale bar: 1 cm, and UV–vis spectrum. The transmittance is over 98% in the entire visible range.

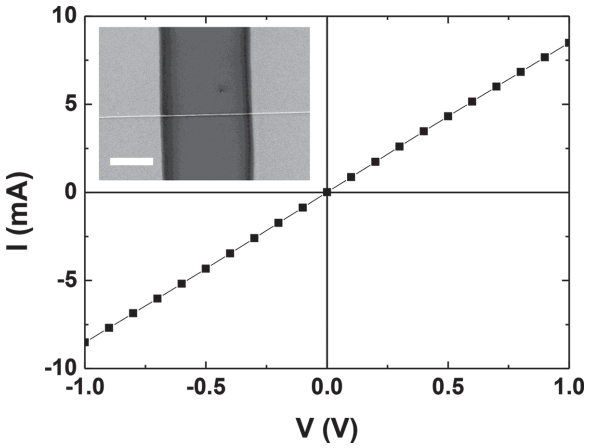

Figure 3. *I–V* curve of single Cu NF aligned between two gold electrodes with a gap of 100 μm (an SEM image of the electrodes/nanofiber is shown in the inset; scale bar: 50 μm).

could contact the NFs, Au contact pads (150 nm) were deposited on the NF array, then a pentacene active layer (50 nm) was thermally evaporated onto two lines of Cu NF electrodes. The channel length of a transistor can be determined and controlled by adjusting the spacing between the Cu NFs. Because these two lines of continuous NFs cannot work as separate individual source and drain electrodes, a cutting process is needed to define each source and drain electrode clearly in an array (Figure 4a). An array of nine pentacene FETs with Cu NF electrodes was successfully fabricated on the Si/SiO_2 substrate (2 cm × 2 cm) with the channel length of 100 μm and channel width of 3 mm (Figures. 4b,c).

The drain current I_D to gate voltage V_G transfer characteristics of the pentacene FET with Cu NF electrodes were measured at drain voltage $V_D = -80$ V for 20 V ≤ V_G ≤ −80 V and showed the behavior of typical pentacene FETs (**Figure 5**a). The device had an on/off current ratio of 7.5×10^6 and a calculated maximum $\mu_{sat} = 0.16$ cm^2 V^{-1} s^{-1} (average $\mu_{sat} \approx 0.1 \pm 0.02$ cm^2 V^{-1} s^{-1}), which is superior to that ($\mu_{sat} = 0.006 \pm 0.0009$ cm^2 V^{-1} s^{-1}) of pentacene FET fabricated using vacuum-deposited Cu film S/D electrodes; this result means that one-dimensional Cu NF electrodes can replace thermally deposited metal-film electrodes. One reason for the superior electrical characteristics of the device with NF electrodes is the existence of Cu oxide species on the NF surface due to chemical instability of Cu. Although Cu oxide inside Cu NFs were reduced during the second calcination process in H_2 atmosphere, perfect removal of all surface oxide species is difficult, so that a small amount of Cu oxide remains after reduction process in H_2 condition.[6] Moreover, Cu NFs are slowly oxidized in ambient condition.[12,13] X-ray photoelectron spectroscopy (XPS) of Cu $2p_{3/2}$ (Figure 5b) supports the existence of Cu oxide species of

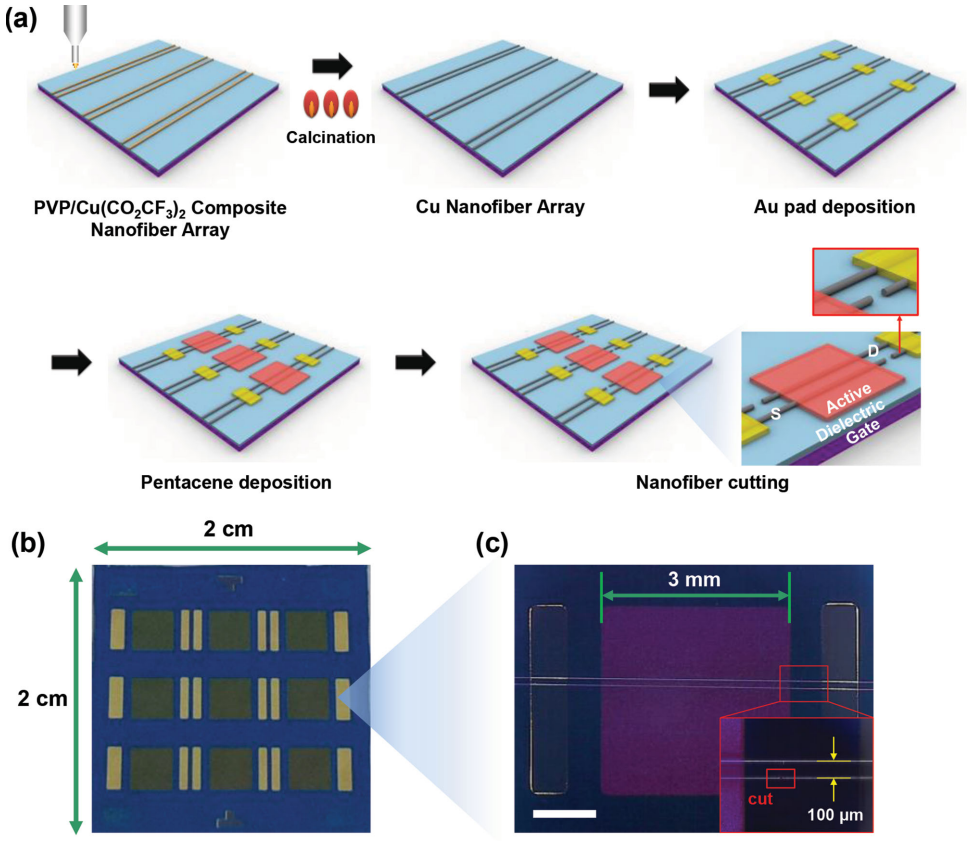

Figure 4. a) Schematic illustration of fabrication procedure for pentacene FET with Cu NF electrode arrays. b) Digital image of pentacene FET array with Cu NF electrode arrays on the Si/SiO_2 substrate (2 cm × 2 cm). c) Digital image of pentacene FET with Cu NF electrode array on the Si/SiO_2 substrate, scale bar, 1 mm (inset: cut part of NF).

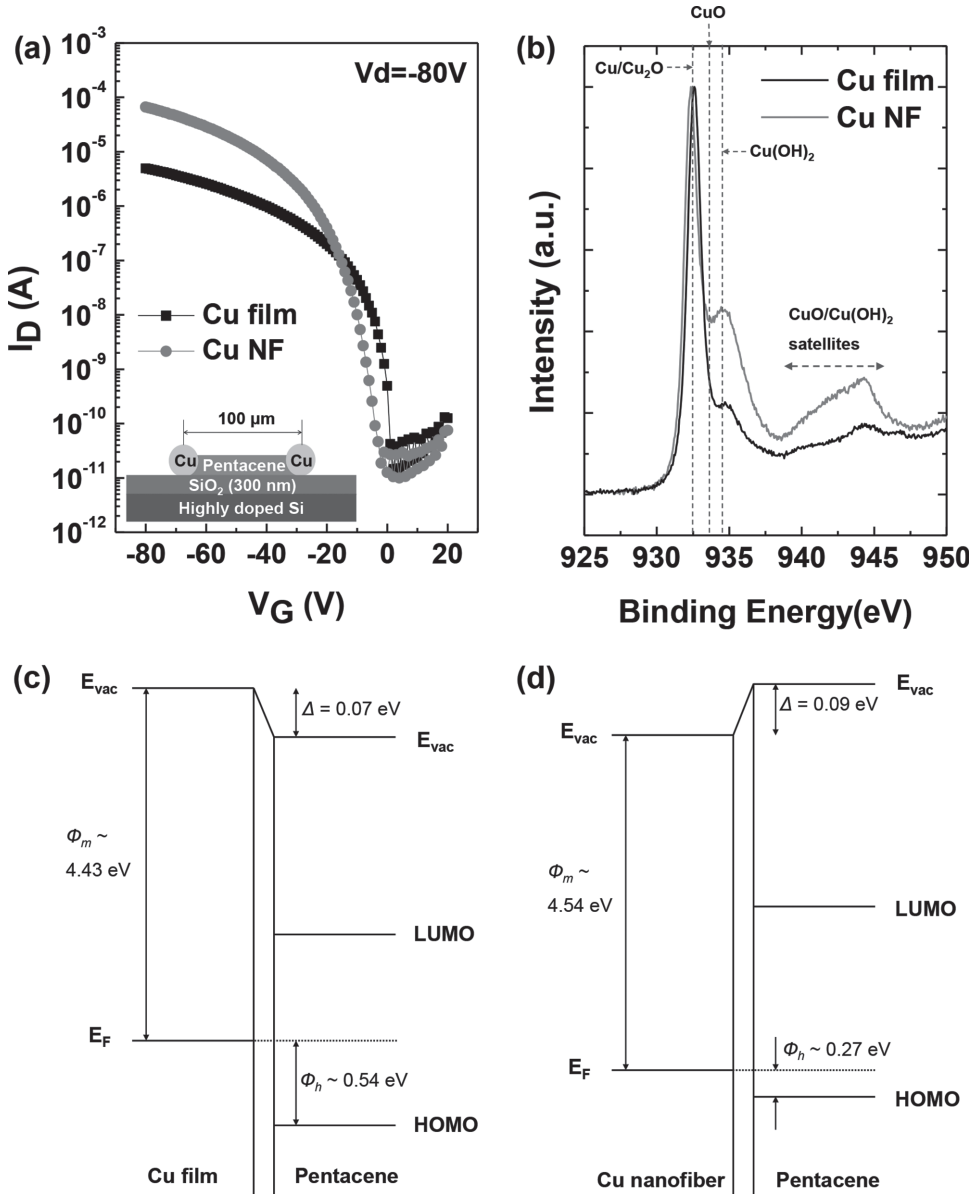

Figure 5. a) Transfer characteristics (inset: specific device structure) of pentacene FETs (channel length = 100 μm, channel width = 3000 μm) with Cu NF electrodes and vacuum-deposited Cu film electrodes. b) Cu $2p_{3/2}$ XPS of Cu NF and Cu film. c,d) Schematic illustration of the energy level diagrams at the interface of Cu film/pentacene (c) and Cu NF/pentacene (d) analyzed using Kelvin probe.

CuO, Cu_2O and $Cu(OH)_2$ on Cu NFs. In comparison to the Cu film, Cu NFs indicated strong intensity peaks at 933.7 (CuO), 934.8 ($Cu(OH)_2$) and 940 to 945 eV ($CuO/Cu(OH)_2$ satellite peaks). A peak at 932.5 eV is the binding energy of both Cu and Cu_2O (**Table 1**). These values are well matched with those reported previously.[24] Cu oxide species are p-type inorganic semiconductors, which have valence band-edge positions of ca. 5.37 (Cu_2O) and ca. 5.42 eV ($CuO/Cu(OH)_2$),[18,25] so the Cu oxides on the surface of the NFs can decrease the hole-injection energy barrier Φ_h between the NF and the pentacene layer by compensating for the low work function Φ_m of the Cu electrode (ca. 4.43 eV, Figure S5, Supporting Information).[19] Φ_h is calculated with consideration of an interfacial dipole Δ as:[26]

$$\Phi_h = IP - \Phi_m - \Delta \quad (1)$$

where IP = 4.9 eV is the ionization potential of pentacene.[27]

Table 1. Cu $2p_{3/2}$ binding energies for Cu and Cu oxide species.

Oxidation state	Cu $2p_{3/2}$ binding energy [eV]
Cu/Cu_2O	932.5
CuO	933.7
$Cu(OH)_2$	934.8
Cu^{2+} satellite peak	944.6

Table 2. Mean values of work function (Φ_m), interfacial dipole (Δ) and injection barrier (Φ_h) of pentacene FETs with vacuum-deposited Cu film electrodes and Cu NF electrodes analyzed by Kelvin probe.

Electrode	Work function [eV]	Interfacial dipole [eV]	Injection barrier [eV]
Cu film	4.43 ± 0.018	−0.07 ± 0.013	0.54 ± 0.013
Cu NF	4.54 ± 0.015	0.09 ± 0.009	0.27 ± 0.009

The energy level alignment at the interfaces of deposited Cu film/pentacene and Cu NF/pentacene was investigated using Kelvin probe (KP) (Figure 5c,d, **Table 2**).[28] To measure the change in Φ_m after pentacene deposition, 5-nm-thick pentacene films were deposited on the Cu film and the Cu NF. The Cu film had Φ_m = 4.43, and the Cu NFs had Φ_m = 4.54 eV; the higher Φ_m of the Cu NF than that of the Cu film is attributed to partial formation of Cu oxide species on the Cu NF surface. After pentacene deposition, the Cu film had Φ_m = 4.36, and the Cu NFs had Φ_m = 4.63 eV. Δ can be determined as the difference between Φ_m before and after pentacene deposition; at the interface of Cu film/pentacene, Δ was −0.07 eV and that of the Cu NF/pentacene interface was 0.09 eV. From Equation 1, the hole injection barrier between the Cu film and pentacene was 0.54 eV, which was higher than that between the Cu NF and pentacene (0.27 eV). This means that holes can be more effectively injected from the Cu NF to pentacene than from the Cu film to pentacene. Therefore, this can partly explain why the μ_{sat} of the FET with the Cu NF electrode was better than the device with the Cu film electrode; another reason may be that the grainy rough surface of NF electrodes increases the contact area with the pentacene active layer, thereby increasing hole injection from electrodes to the active layer.[20,29] Although the device with Cu NF electrodes had higher carrier mobility μ than the device with Cu film electrodes, a non-Ohmic contact still appeared in the I_D–V_D output characteristics curve (Figure S6, Supporting Information) due to the contact resistance r_c.

Pentacene grains near and on the Cu NF electrodes are smaller than those on the SiO_2 dielectric (Figure S7, Supporting Information) due to the poor compatibility between the rough surface of the Cu NF electrodes and pentacene active layer. To decrease r_c, we modified the surface of Cu NF with Trichloro(1H,1H,2H,2H-perfluorooctyl)silane (FOTS) which forms a self-assembled monolayer. Because FOTS has fluorine moieties at the end group of the molecules it increases the Φ_m of metal electrodes; [30,31] this means that the injection barrier between Cu NF electrode and pentacene is decreased. FOTS modification improved the contact from S-shaped non-Ohmic contact to linear Ohmic contact in the device with modified Cu NF electrodes (Figure S8, Supporting Information). In the linear regime of the transfer curve of the device with modified Cu NF electrodes, linear carrier mobility μ_{lin} = 0.06 ± 0.006 $cm^2 V^{-1} s^{-1}$ at V_D = −10 V, which is almost an order of magnitude higher than in the device with pristine Cu NF electrodes (μ_{lin} = 0.008 ± 0.0011 $cm^2 V^{-1} s^{-1}$) (Figure S8, Supporting Information). The threshold voltage V_{th} was increased because FOTS induced additional carrier accumulation in the channel; this accumulation supplemented the external gate field of the FET.[32] The same phenomenon appeared in a pentacene FET with deposited Cu film S/D electrodes (Figure S9, Supporting Information). In the linear region, μ_{lin} increased from 0.0019 ± 0.0007 $cm^2 V^{-1} s^{-1}$ in the device with pristine Cu film electrode to 0.017 ± 0.0025 $cm^2 V^{-1} s^{-1}$ in the device with modified Cu film electrode at V_D = −10 V (Figure S9, Supporting Information). These results are consistent with the KP results of Φ_m in pristine Cu NFs and FOTS-modified NFs (Figure S10, Supporting Information).

In summary, we printed large-scale-aligned Cu NF arrays that have constant spacing in a large area and used the printed single-stranded Cu NFs themselves as S/D nanoelectrodes in organic transistors. The Cu NF had an electrical resistivity of 14.1 μΩ cm, which is slightly higher than that of bulk Cu. Fabricated bottom-contact pentacene FET arrays that used pristine single-stranded Cu NFs as S/D electrodes had a maximum field-effect hole mobility of 0.16 $cm^2 V^{-1} s^{-1}$ and an on/off current ratio of 7.5×10^6. This result implies that one-dimensional Cu NF electrodes can replace thermally deposited metal-film electrodes that decrease the total transmittance of the device arrays, and thus significantly improve the total transmittance of electronic device arrays, rendering them more suitable for transparent electronics. This is the first demonstration and device application of individually position-controllable, large-scale-aligned nanosized Cu fibers as one-dimensional wire-type electrodes, which represents a significant advance over the conventional randomly coiled sheet-type metal fiber electrodes, in that our strategy significantly improves the transmittance, position addressability, and compatibility with large-area device array fabrication. The feasibility of using Cu NF arrays as nanoelectrodes also proves that our strategy will be promising for fabrication of various next-generation large-area nanoelectronics in a controlled manner.

Experimental Section

EHD Nanowire Printing: All the binding polymers and Cu precursors were purchased from Sigma–Aldrich. Polyvinylpyrrolidone (PVP) (MW = 1.3×10^6 g mol^{-1}, Aldrich) and Cu(II) trifluoroacetate ($Cu(CO_2CF_3)_2$) (Aldrich) were dissolved in a solvent mixture (1:1 w:w) of N,N-dimethylformamide (Aldrich) and tetrahydrofuran (Samchun Chemical). The concentration of PVP was 9% (w:w) and that of $Cu(CO_2CF_3)_2$ was 23% (w:w). The mixed solution was stirred for 3 h at 500 rpm at room temperature to form a viscous and homogeneous transparent blue solution. The PVP/$Cu(CO_2CF_3)_2$ solution was loaded in a 500-μL glass syringe (Hamilton) with a stainless-steel nozzle tip (inner diameter = 100 μm), and applied at a steady flow rate of 100 nL/min and external voltage of 0.5 kV, which initiated a continuous liquid jet at the end of nozzle tip. While the liquid jet arrived at the surface of silicon wafer on a flat, grounded collector, the liquid jet was stretched by the external electric field and solidified by evaporation of solvent; the resulting NF on the substrate was a few hundred nanometers in diameter. The tip-to-collector distance was 7 mm. By moving the collector laterally at 58.3 cm s^{-1}, a parallel NF array was printed on the substrate. Randomly oriented NF mats were obtained using same solution with experimental parameters of flow rate of 500 nL/min, external voltage of 3.2 kV, and tip-to-collector distance of 15 cm. During the first calcination process, printed PVP/$Cu(CO_2CF_3)_2$ composite NF array was annealed in air at 500 °C for 1 h. The second calcination used rapid thermal annealing at 300 °C for 1 h in H_2 gas at a gas flow rate of 200 sccm. These processes enabled fabrication of an individually position addressable, large-scale-aligned Cu NF array.

Pentacene Field-Effect Transistor: To enable contact between the measuring probe tip and Cu NF electrodes, an Au pad (150 nm) was deposited on the Cu NF array using a thermal evaporation system and metal shadow masks. NFs were cut using the measuring probe tip to define S/D electrodes. Pentacene films (Polysis) (50 nm) and Cu film electrodes (150 nm) were thermally deposited through metal shadow masks in high vacuum (5×10^{-6} Torr). Device performance analysis was conducted under an N_2 atmosphere.

Self-Assembled Monolayer Modification: Trichloro(1H,1H,2H,2H-perfluorooctyl)silane (FOTS) ($CF_3(CF_2)_5CH_2CH_2SiCl_3$, Aldrich) was deposited on the Cu NFs, the Cu film, and the SiO_2 surface by vaporization for 2 h.

Characterization: The characteristics of the Cu NFs and the pentacene FETs were measured by digital microscopy (DIMIS-M), optical microscopy (Olympus), scanning electron microscopy with energy-dispersive X-ray spectroscopy (XL30S FEG, Philips electron optics B.V), atomic force microscopy (Tecsco), UV–vis spectrometry (S-3100, SCINCO), X-ray photoelectron spectroscopy (AXIS-NOVA, Kratos Inc), X-ray diffraction (Rigaku), and high-resolution transmission electron microscopy (JEOL), as well as by using a Kelvin probe system (SKP5050, Kelvin Probe Technology, Ltd., Wick, UK), a Probe station (MS-Tech), and a semiconductor characterization system (Keithley 4200) under N_2 in a glove box. For the resistivity measurements, Au was thermally deposited using a metal shadow mask on a single Cu NF. To measure the I_D–V_G transfer curve of pentacene FET, the V_D was −10 V for the linear region and −80 V for the saturation region. Sweep ranges of V_G were from 20 V to −80 V for the devices with pristine electrodes and from 60 V to −80 V for the devices with FOTS modified electrodes. In the I_D–V_G output curve, V_G was decreased from 0 V to −80 V in increments of −10 V for the devices with pristine electrodes and from 60 V to −80 V in increments of −20 V for the devices with FOTS modified electrodes, and the sweep range of V_D was from 0 V to −80 V.

Supporting Information

Supporting Information is available from the Wiley Online Library or from the author.

Acknowledgements

This work was supported by the Center for Advanced Soft-Electronics funded by the Ministry of Science, ICT and Future Planning as Global Frontier Project (2014M3A6A5060947). This work was also supported by Basic Science Research Program through the National Research Foundation of Korea (NRF) funded by the Ministry of Education (NRF- 2013R1A1A2012660).

Received: August 5, 2014
Revised: September 11, 2014
Published online: October 29, 2014

[1] a) B. H. Hong, S. C. Bae, C.-W. Lee, S. Jeong, K. S. Kim, *Science* **2001**, *294*, 348; b) Y. Wu, J. Xiang, C. Yang, W. Lu, C. M. Lieber, *Nature* **2004**, *430*, 61; c) Y. Sun, B. Gates, B. Mayers, Y. Xia, *Nano Lett.* **2002**, *2*, 165; d) S. H. Liu, J. B. H. Tok, Z. Bao, *Nano Lett.* **2005**, *5*, 1071; e) Y. Sun, B. Mayers, T. Herricks, Y. Xia, *Nano Lett.* **2003**, *3*, 955; f) U. Jeong, P. H. C. Camargo, Y. H. Lee, Y. Xia, *J. Mater. Chem* **2006**, *16*, 3893.

[2] a) J.-Y. Lee, S. T. Connor, Y. Cui, P. Peumans, *Nano Lett.* **2008**, *8*, 689; b) W. Gaynor, G. F. Burkhard, M. D. McGehee, P. Peumans, *Adv. Mater.* **2011**, *23*, 2905; c) M.-S. Lee, K. Lee, S.-Y. Kim, H. Lee, J. Park, K.-H. Choi, H.-K. Kim, D.-G. Kim, D.-Y. Lee, S. W. Nam, J.-U. Park, *Nano Lett.* **2013**, *13*, 2814.

[3] a) D. O. Shin, J. H. Mun, G.-T. Hwang, J. M. Yoon, J. Y. Kim, J. M. Yun, Y.-B. Yang, Y. Oh, J. Y. Lee, J. Shin, K. J. Lee, S. Park, J. U. Kim, S. O. Kim, *ACS Nano* **2013**, *7*, 8899; b) J. Y. Kim, B. H. Kim, J. O. Hwang, S.-J. Jeong, D. O. Shin, J. H. Mun, Y. J. Choi, H. M. Jin, S. O. Kim, *Adv. Mater.* **2013**, *25*, 1331; c) B. H. Kim, Y. Choi, J. Y. Kim, H. Shin, S. Kim, S. -W. Son, S. O. Kim, P. Kim, *Adv. Mater.* **2014**, *26*, 4665.

[4] J.-U. Park, M. Hardy, S. J. Kang, K. Barton, K. Adair, D. K. Mukhopadhyay, C. Y. Lee, M. S. Strano, A. G. Alleyne, J. G. Georgiadis, P. M. Ferreira, J. A. Rogers, *Nat. Mater.* **2007**, *6*, 782.

[5] S. Jeong, H. C. Song, W. W. Lee, H. J. Suk, S. S. Lee, T. Ahn, J.-W. Ka, Y. Choi, M. H. Yi, B.-H. Ryu, *J. Mater. Chem.* **2011**, *21*, 10619.

[6] S. Jeong, S. H. Lee, Y. Jo, S. S. Lee, Y.-H. Seo, B. W. Ahn, G. Kim, G.-E. Jang, J.-U. Park, B.-H. Ryu, Y. Choi, *J. Mater. Chem. C* **2013**, *1*, 2704.

[7] S. Jeong, K. Woo, D. Kim, S. Lim, J. S. Kim, H. Shin, Y. Xia, J. Moon, *Adv. Funct. Mater.* **2008**, *18*, 679.

[8] a) D. Kim, S. Jeong, H. Shin, Y. Xia, J. Moon, *Adv. Mater.* **2008**, *20*, 3084; b) J. Perelaer, B. J. de Gans, U. S. Schubert, *Adv. Mater.* **2006**, *18*, 2101; c) T.-W. Lee, Y. Byun, B.-W. Koo, I.-N. Kang, Y.-Y. Lyu, C. H. Lee, L. Pu, S. Y. Lee, *Adv. Mater.* **2005**, *17*, 2180; d) D. Sung, A. de la Fuente Vornbrock, V. Subramanian, *IEEE Trans. Compon. Packag. Technol.* **2010**, *33*, 105; e) M. M. Voigt, A. Guite, D. Y. Chung, R. U. A. Khan, A. J. Campbell, D. D. C. Bradley, F. S. Meng, J. H. G. Steinke, S. Tierney, I. McCulloch, H. Penxten, L. Lutsen, O. Douheret, J. Manca, U. Brokmann, K. Sonnichsen, D. Hulsenberg, W. Bock, C. Barron, N. Blankaert, S. Springer, J. Grupp, A. Mosley, *Adv. Funct. Mater.* **2010**, *20*, 239; f) J. Noh, D. Yeom, C. Lim, H. Cha, J. Han, J. Kim, Y. Park, V. Subramanian, G. Cho, *IEEE Trans. Electron. Packag. Manuf.* **2010**, *33*, 275.

[9] H. Wu, D. Lin, R. Zhang, W. Pan, *Chem. Mater.* **2007**, *19*, 1895.

[10] M. Bognitzki, M. Becker, M. Graeser, W. Massa, J. H. Wendorff, A. Schaper, D. Weber, A. Beyer, A. Golzhauser, A. Greiner, *Adv. Mater.* **2006**, *18*, 2384.

[11] H. Xiang, Y. Long, X. Yu, X. Zhang, N. Zhao, J. Xu, *CrystEngComm* **2011**, *13*, 4856.

[12] H. Wu, L. B. Hu, M. W. Rowell, D. S. Kong, J. J. Cha, J. R. McDonough, J. Zhu, Y. A. Yang, M. D. McGehee, Y. Cui, *Nano Lett.* **2010**, *10*, 4242.

[13] H. Wu, D. Kong, Z. Ruan, P. C. Hsu, S. Wang, Z. Yu, T. J. Carney, L. Hu, S. Fan, Y. Cui, *Nat. Nanotechnol.* **2013**, *8*, 421.

[14] a) M. Park, J. Im, M. Shin, Y. Min, J. Park, H. Cho, S. Park, M.-B. Shim, S. Jeon, D.-Y. Chung, J. Bae, J. Park, U. Jeong, K. Kim, *Nat. Nanotechnol.* **2012**, *7*, 803; b) S.-Y. Min, J. Bang, J. Park, C.-L. Lee, S. Lee, J.-J. Park, U. Jeong, S. Kim, T.-W. Lee, *RSC Adv.* **2014**, *4*, 11585; c) H. Cho, S.-Y. Min, T.-W. Lee, *Macromol. Mater. Eng.* **2013**, *298*, 475.

[15] S. H. Choi, T. S. Hyun, H. J. Lee, S. Y. Jang, S. G. Oh, I.-D. Kim, *Electrochem. Solid-State Lett.* **2010**, *13*, A65.

[16] H. Lee, S. H. Choi, S. M. Jo, D. Y. Kim, S. Kwak, M. W. Cha, I.-D. Kim, S. Y. Jang, *J. Phys. D: Appl. Phys.* **2009**, *42*, 125409.

[17] D.-J. Yun, S.-H. Lim, S.-H. Cho, B.-S. Kim, S.-W. Rhee, *J. Electrochem. Soc.* **2009**, *156*, H634.

[18] C.-a. Di, G. Yu, Y. Q. Liu, Y. L. Guo, Y. Wang, W. P. Wu, D. B. Zhu, *Adv. Mater.* **2008**, *20*, 1286.

[19] Y. Su, M. Wang, F. Xie, J. Chen, W. Xie, N. ZhaoJ. Xu, *Org. Electron.* **2013**, *14*, 775.

[20] C. A. Di, G. Yu, Y. Q. Liu, Y. L. Guo, W. P. Wu, D. C. Wei, D. B. Zhu, *Phys. Chem. Chem. Phys.* **2008**, *10*, 2302.

[21] S.-Y. Min, T.-S. Kim, B. J. Kim, H. Cho, Y. -Y. Noh, H. Yang, J. H. ChoT.-W. Lee, *Nat. Commun.* **2013**, *4*, 1773.

[22] W. Xu, H.-K. Seo, S.-Y. Min, H. Cho, T.-S. Lim, C.-y. Oh, Y. Lee, T.-W. Lee, *Adv. Mater.* **2014**, *26*, 3459.

[23] E. Villamor, M. Isasa, L. E. Hueso, F. Casanova, *Phys. Rev. B* **2013**, *87*, 094417.
[24] a) I. Platzman, R. Brener, H. Haick, R. Tannenbaum, *J. Phys. Chem. C* **2008**, *112*, 1101; b) J. Hernandez, P. Wrschka, G. S. Oehrlein, *J. Electrochem. Soc.* **2001**, *148*, G389; c) T. Waechtler, S. Oswald, N. Roth, A. Jakob, H. Lang, R. Ecke, S. E. Schulz, T. Gessner, A. Moskvinova, S. Schulze, M. Hietschold, *J. Electrochem. Soc.* **2009**, *156*, H453; d) N. S. Mclntyre, M. G. Cook, *Anal. Chem.* **1975**, *47*, 2208.
[25] a) F. P. Koffyberg, F. A. Benko, *J. Appl. Phys.* **1982**, *53*, 1173; b) H.-H. Strehblow, V. Maurice, P. Marcus, *Electrochim. Acta* **2001**, *46*, 3755; c) U. Collisi, H. -H. Strehblow, *J. Electroanal. Chem.* **1990**, *284*, 385.
[26] H. Ishii, K. Sugiyama, E. Ito, K. Seki, *Adv. Mater.* **1999**, *11*, 605.
[27] N. J. Watkins, L. Yan, G. Yongli, *Appl. Phys. Lett.* **2002**, *80*, 4384.
[28] S. Lee, G. Jo, S. J. Kang, G. Wang, M. Choe, W. Park, D. Y. Kim, Y. H. Kahng, T. Lee, *Adv. Mater.* **2011**, *23*, 100.
[29] C. A. Di, Y. Q. Liu, G. Yu, D. B. Zhu, *Acc. Chem. Res.* **2009**, *42*, 1573.
[30] I. H. Cambell, J. D. Kress, R. L. Martin, D. L. Smith, N. N. Barashkov, J. P. Ferraris, *Appl. Phys. Lett.* **1997**, *71*, 3528.
[31] I. H. Campbell, S. Rubin, T. A. Zawodzinski, J. D. Kress, R. L. Martin, D. L. Smith, *Phys. Rev. B* **1996**, *54*, R14321.
[32] S. Kobayashi, T. Nishikawa, T. Takenobu, S. Mori, T. Shimoda, T. Mitani, H. Shimotani, N. Yoshimoto, S. Ogawa, Y. Iwasa, *Nat. Mater.* **2004**, *3*, 317.